

47(2), pp. 57-69, 2016

DOI: 10.3311/PPar.9478

Creative Commons Attribution 

Dániel Bakonyi^{1*}, Gergely Dobszay¹

RESEARCH ARTICLE

Received 13 May 2016; accepted 18 July 2016

Abstract

As the literature does not contain enough measurement data to create dedicated correlations for the Nusselt number and convective heat transfer inside box type windows, CFD simulations are performed to study the type of natural convection in such windows. Validation is attempted with the help of the turbulence benchmark of Betts and Bokhari (2000) and comparison with other simulations found in the literature. The $k-\omega$ SST model of Menter (1994) is selected to perform a wide range study of the cavity aspect ratios and Rayleigh numbers expected in box windows, enabling an analysis of the types of convections encountered. A new correlation is introduced to calculate the convective heat transfer, and finally, the study is augmented to investigate the effects the temperature stratification has on critical glazing surface temperatures.

Keywords

historical double skin window, box type window, heat loss calculation, convection in glazing cavity, natural convection

1 Introduction

The first part of this article showed that the large cavity dimensions of traditional double skin box type windows result in a type of natural convection very different from the one encountered in the much thinner cavities of insulating glass units (henceforth IG units). Most of our current tools for calculating fenestration heat transfer were developed for contemporary single skin windows with IG units. This raises questions regarding the validity of said methods for the case of box type windows. One key area to be investigated is the correlations used in these calculations for predicting the Nusselt number and the convective heat transfer coefficient in the glazing cavity. The correlations in the most commonly used standards EN 673 (2011) and ISO 15099 (2003) for glazing area heat transfer seem inadequate. They both neglect the cavity aspect ratio dependence of the Nusselt number (which is an influencing parameter reported by many other sources for small aspect ratio cavities), and box type windows simply lie outside their published area of validity. If we use them regardless, they show significant disagreement with more recent results as reported in part one of this article. Based on the available literature alone, no definitive statement can be made on which other correlation is best suited for box type windows.

A new dedicated study focusing directly on the flow regime encountered in box type windows is needed. A schematic representation of the cavity geometry, dimensions and boundary conditions of the problem is found in Fig. 1. The flow type or flow regime is described by two dimensionless numbers: the aspect ratio, which is defined as the height to width ratio of the vertical section of the cavity $A = H/L$, and the Rayleigh number, which is the product of the Prandtl and Grashof numbers $Ra = Gr \cdot Pr$, calculated based on the cavity thickness. For a box window, we have to investigate cavities with $A = 7$ to 35 [-], which is much smaller, and $Ra = 6e5$ to $3e7$ [-], which is much bigger than in IG units.

In the literature, besides a few analytical papers, we find studies based mainly on either laboratory measurements or Computational Fluid Dynamics simulations. A good review of some of the available convective heat transfer measurement data is

¹ Department of Building Constructions,
Faculty of Architecture,
Budapest University of Technology and Economics,
H-1111, Budapest, Műegyetem rkp. 3., Hungary

* Corresponding author, e-mail: dbakonyi@epsz.bme.hu

found in Ganguli et al. (2009). Good measurement setups are very difficult to construct as the heat flux, temperature differences, and velocities to be recorded are all quite small, and the required boundary conditions can be hard to achieve in a way that they do not interfere with the measurement accuracy, especially in the case of the convective heat flow. Ecker and Carlson (1961) used interferometry to measure the temperature field in cavities but did not reach Rayleigh numbers high enough to be useful for box windows. The measurements of Yin et al. (1978) focused on the aspect ratio range of $4.9 < A < 78.7$ [-] and Rayleigh numbers of $1e4 < Ra < 7e6$ [-], which extends well into the range of interest for our current study. However, as Ganguli et al. (2009) noted, the concentration of heat transfer to the top and bottom edges of the cavity for low aspect ratios raises questions regarding the accuracy of the heat flux measurement methods they used. ElSherbiny et al. (1982) conducted one of the most comprehensive and most cited measurement campaigns in the literature about the natural convection in rectangular cavities. They investigated the effect the treatment of the side wall boundary conditions have on measurement results. They used a high conductivity material to form the side walls of their measurement setup resulting in a near linear temperature profile, which is a standard practice for most such measurements. While this is a good fit for flows in the conduction regime where the temperature gradient in the fluid is itself linear, which results in essentially no sideways heat flux, it complicates matters when a boundary layer regime flow is investigated. Here, especially at the top and bottom zones of the cavity, the core of the fluid is close to either the cold or the hot boundary temperature while the solid wall of the cavity tries to enforce a linear temperature profile. This leads to nonzero sideways heat flux possibly causing difficulties when using the data for validation. Zhao (1997) noted that ElSherbiny's data shows an unphysical tendency for large Ra and small A numbers. According to theory, the overall heat transfer coefficient should decrease with increasing aspect ratio for any given Ra number as the top and bottom corners of the cavity, where the convection cell loops around and the heat transfer is more intense, get further apart and their effect gets proportionally smaller in the overall heat transfer. The data of ElSherbiny shows the opposite trend, indicating a possible measurement error for highly stratified low aspect ratio flows. Shewen et al. (1996) have developed a new method for the simultaneous heating or cooling of, and heat flux measurement on cavity walls in experimental apparatus aimed at the study of natural convection in rectangular cavities based on the Peltier effect. Unfortunately, their study concentrated on cavities with aspect ratios of 40 [-] or larger and Rayleigh numbers less than $1e6$ [-]. At the moment, there is no dataset in the literature that covers the entire aspect ratio and Rayleigh number range of flows in box type windows with sufficient resolution and is pronounced reliable by most of the sources to serve as a basis for a new correlation. We have to turn to CFD simulations instead.

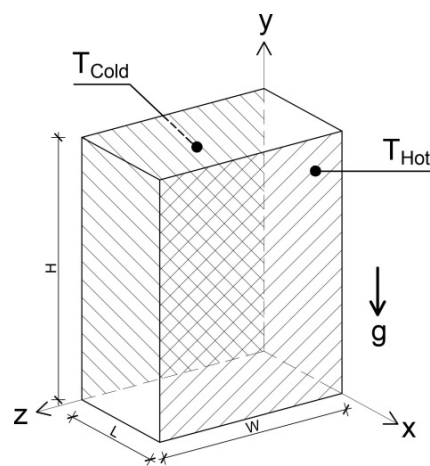


Fig. 1 A schematic representation of the ‘natural convection in a rectangular differentially heated cavity’ problem

With advancements in numerical methods and computational resources, most newer studies rely heavily on CFD. While earlier works were limited to laminar flows such as the work of Newell and Schmidt (1970), Raithby and Wong (1981), Lee and Korpela (1983), Wright and Sullivan (1993) and Zhao (1997), the type of natural convection in the cavities of box type windows is in the fully turbulent boundary layer regime. The choice of turbulence model is thus a key issue, and the results have to be thoroughly validated. From the main approaches to turbulence modelling: RANS (Reynolds-Averaged Navier-Stokes), LES (Large Eddy Simulation) and DNS (Direct Numerical Simulation) methods RANS models will be investigated, as a great number of individual simulations will be required to adequately resolve the flow regime of box type windows and to later model entire complex window assemblies at an acceptable computational cost.

There are few datasets available in the literature that are intended to aid the validation of turbulence models for natural convection problems in enclosed rectangular cavities. The study best suited for box type windows is that of Betts and Bokhari (2000), made available for researchers through the ERCOFTAC website. Betts and Bokhari conducted their measurements by modifying an earlier apparatus of Dafa’Alla and Betts (1996). The test rig enclosed an air-filled cavity of 2.18 [m] height, 0.076 [m] thickness and 0.52 [m] length. The temperature difference was applied by the 2.18x0.52 [m] vertical walls that were constructed from polished aluminium with water jackets for cooling or heating, together with a supporting wooden frame and thermal insulation towards the outside. The aim of the design was to create truly isothermal conditions on the cold and warm sides. This was achieved, among other things, by slightly extending the walls beyond the cavity in a vertical direction. The side walls were created from a rubber material with a thermal conductivity near the effective conductance of the cavity ($\lambda=0.155$ [W/mK]). A series of

thermocouples were embedded in these rubber walls. They measured a near linear temperature profile in the side walls between the hot and cold aluminium walls without the excessive heat flows of much better conducting walls that were used in many earlier measurements. The flow cavity had an aspect ratio of $A=28.68$ [-] and measurements were conducted at Rayleigh numbers of $Ra=0.86e6$ and $1.43e6$ [-] by varying the temperature difference ($\Delta T=19.6$ and 39.9 [$^{\circ}C$]). Although the aspect ratio is at the higher, and the Rayleigh number (for the bigger temperature difference) at the lower end of the range found in box type windows, the results show a very similar turbulent boundary layer flow. Betts and Bokhari reported both the time averaged mean, and the root mean square of the temperature and flow velocities (both horizontal and vertical components) throughout the cavity along predetermined horizontal and vertical sections (see Fig. 2). The temperature measurements were done with a 75 [μm] diameter K type traversing thermocouple with a response time of 0.07 [s], a position accuracy less than the thermocouple diameter, and a digital accuracy of 0.1 [$^{\circ}C$]. Laser Doppler anemometry (LDA) was used for the velocity measurements. Due to the construction of their setup and the nature of the stratified boundary layer flows, the convective heat transfer could not be measured directly. Instead, they only reported local heat flux densities calculated based on the measured wall-normal temperature gradients in the laminar sublayer at discrete points: $q_{local} = \lambda_{air} * \partial T / \partial n$. An average Nusselt number is also given calculated from the local heat flux densities.

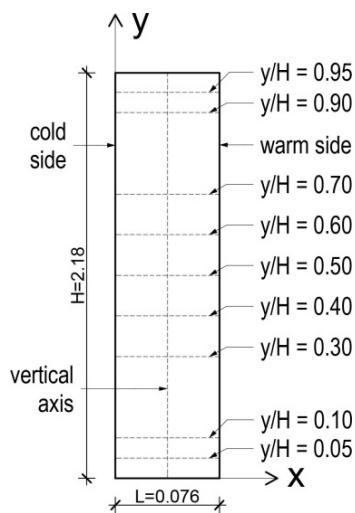


Fig. 2 A schematic representation of the ‘natural convection in a rectangular differentially heated cavity’ problem

Betts and Bokhari (2000) reported an effectively 2D temperature field for 90% of the cavity width. The velocity field could only be measured for the middle 50% of the cavity where it was also found to be near perfectly 2D. Both velocity and temperature profiles were antimetric. In the core, the velocity is near zero, but the velocity fluctuations are the strongest

(70% of the mean velocity near the walls) due to the interaction of the rising and sinking boundary layers. Peak velocities were found along the bottom of the hot ($y/H=0.1$ [-]) and the top of the cold ($y/H=0.9$ [-]) walls in the rising and sinking boundary layers. The temperature field also showed strong boundary layers next to the two vertical walls, with a near zero horizontal gradient in the core. The top and bottom ends of the cavity showed strong vertical temperature stratification while the middle portion of the cavity did not.

The data of Betts and Bokhari has since been used by many researchers for testing turbulence models. Hsieh and Lien (2004) studied low-Re $k-\epsilon$ models for weakly turbulent flows with an unsteady RANS solver. Unlike some other flows, the turbulent boundary layer flow in the benchmark of Betts and Bokhari proved sufficiently turbulent to allow for a steady-state solution without the extra computational strain of a transient simulation. They conducted a mesh refinement study but found little difference between their 50×100 , 75×150 and 100×200 non-uniform rectangular grids, except in the laminar-turbulent transition point in the boundary layers. Finer resolutions in the longitudinal (vertical) direction gave slightly smaller Nusselt numbers. They also investigated the effect of different treatments of the buoyancy source in the turbulent kinetic energy equation, including the case of a zero buoyancy source, and found little to no difference indicating that the term is negligible. Although the temperature and velocity results were good, the Lien and Leschziner $k-\epsilon$ model (1999) underpredicted the average Nu number by 20% compared to Betts and Bokhari (see Table 1).

Zhang et al. (2007a; 2007b) tested the zero equation models of Chen and Xu (1998), the RNG $k-\epsilon$ model of Yakhot and Orszag (1986), the low-Re $k-\epsilon$ model of Launder and Sharma (1974), the SST $k-\omega$ model of Menter (1994), the modified $v2f$ model of Davidson et al. (2003), the Reynolds Stress Model of Gibson and Launder (1978) as well as Detached Eddy (DES) and Large Eddy Simulations (LES), among other benchmarks, for the turbulent natural cavity-convection problem. They used a non-uniform rectangular mesh with $y^+ \leq 0.3$ for RANS and 0.1 for DES and LES models. The grid dependence study found no need for further refinement. The zero equation and DES models both performed badly and predicted erroneous velocity fields, while the low-Re $k-\epsilon$ model had trouble predicting the temperature field at the top and bottom ends of the cavity. The RNG SST and RSM models all gave comparably good results and the $v2f$ model of Davidson achieved the best fit with the measurements. Aksouh et al. (2010) compared simulations with the RNG $k-\epsilon$ and SST $k-\omega$ models with the data of Betts and Bokhari on two and three-dimensional non-uniform rectangular grids; they found the SST model to give superior results for heat transfer, and the difference between 2 and 3D calculations negligible. Their calculated average Nusselt number was within 10% of the one reported by Betts and Bokhari (although this is not born out by the figure they published

Table 1 Comparison of calculated Nu numbers compared to the measurements of Betts and Bokhari

source	software	mat. prop.	buoyancy	turb. model	Ra=0.86e6 [-] (Nu _{BB} =5.85 [-])		Ra=1.43e6 [-] (Nu _{BB} =7.57 [-])	
					Nu	%Err	Nu	%Err
Hsieh and Lien	?		Boussinesq	low-Re k-ε LL (Lien and Leschziner, 1999)	-	-	5.99	-20.87%
Aksouh et al.	?		Boussinesq	k-ω SST	5.51	-5.8%	6.96	-8.06%
Ammour et al.	Code-Saturn	const.	Boussinesq	k-ω SST	5.266	-10%	-	-
El Moutaouakil et al. (2014)	custom code	const.	Boussinesq	k-ω SST	5.53	-5.47%	6.687	-11.66%

for the local Nusselt numbers distribution). In a later article, Aksouh et al. (2011) revised their results slightly by stating that the three-dimensional effect might, after all, be important for the flow, at least at the very bottom and top ends of the cavity. They also proposed a correlation for the Nusselt number, but only as a function of the Rayleigh number and for the singular aspect ratio of the investigated A=28.68 [-]. Keyn and Agarwal (2013) performed a similar study comparing the realizable k-ε and k-ω SST models, with results also favouring the latter. Ammour et al. (2011) ran unsteady simulations with the standard k-ε, k-ω SST, v2f, φ-f and RSM RANS turbulence models for the lower Ra number case of Betts and Bokhari. They achieved good results with low-Re models and also found the v2f to give the best results, though at the cost of occasional numerical instabilities. Another study of some 20 eddy-viscosity turbulence models based on Betts and Bokhari is found in El Moutaouakil et al. (2014). Regarding both accuracy and total computational time, they found the v2f, k-ω SST and the φ-f models as the best choice. The average Nusselt number they calculated with these models fell within 10% of the one predicted by Betts and Bokhari.

A number of other publication could also be cited using the data of Betts and Bokhari, but unlike the ones reviewed here, most other works are limited to studying the difference between the calculated and measured temperature and velocity fields and do not give an analysis of the convective heat transfer. The calculated Nusselt numbers found in the literature are summed up in Table 1. Unfortunately, although many sources found a good qualitative agreement between the overall calculated and measured temperature and velocity fields, the Nusselt number predictions show larger discrepancies.

2 CFD model

Based on the literature review, a two-dimensional steady state model was built with the turbulence modelling based on the Reynolds Averaged Navier-Stokes equations. The program ANSYS FLUENT release 13.0 (2010) was used for all of the CFD simulations. For the buoyancy forces, both the Boussinesq approximation and the incompressible ideal gas formulation was tested, with little-to-no difference between the results.

In the end, the ideal gas model was used. The continuity equation (in Cartesian tensor notation) can thus be expressed as:

$$\frac{\partial}{\partial x_i}(\rho \bar{u}_i) = 0 \quad (1)$$

where: ρ [kg/m³] – the density
 \bar{u}_i [m/s] – the ith component of the mean velocity vector

Which is solved with the help of the ideal gas law:

$$\rho = \frac{P_{op}}{R} \frac{1}{T} \quad (2)$$

where: ρ [kg/m³] – the density
 P_{op} [Pa] – the operative pressure (101325 [Pa])
 R [J/molK] – the universal gas constant
 M_w [kg/mol] – the molecular mass of the fluid (air)
 T_m [K] – the mean temperature

The momentum equation:

$$\frac{\partial(\rho \bar{u}_i \bar{u}_j)}{\partial x_j} = -\frac{\partial \bar{P}}{\partial x_j} + \frac{\partial}{\partial x_j} \left(\mu \frac{\partial \bar{u}_i}{\partial x_j} - \rho \overline{u'_i u'_j} \right) - \rho g \quad (3)$$

where: ρ [kg/m³] – the density
 \bar{u}_j [m/s] – the jth component of the mean velocity vector
 \bar{P} [Pa] – the mean pressure
 μ [Ns/m²] – the dynamic viscosity
 u'_j [m/s] – the jth component of the fluctuating velocity
 g [m/s²] – the gravitational acceleration

The Reynolds stresses are calculated by one of the following turbulence models:

- the k-ω SST model of Menter (1994)
- the RNG k-ε model
- the realizable k-ε model

- the low-Re k-ε model of Abid (1993)
- the low-Re k-ε model of Lam-Bremhost (1981)
- the low-Re k-ε model of Launder and Sharma (1974)
- the v2f model of Durbin (1995)

The energy equation takes the following form:

$$\frac{\partial(\rho c_p \bar{u}_i T_m)}{\partial x_i} = \frac{\partial}{\partial x_i} \left(\lambda \frac{\partial T_m}{\partial x_i} + \frac{v_t}{\sigma_t} \frac{\partial T_m}{\partial x_i} \right) \quad (4)$$

where: ρ [kg/m³] – the density
 c_p [J/kgK] – the specific heat capacity
 u_i [m/s] – the i^{th} component of the mean velocity vector
 T_m [K] – the mean temperature
 λ [W/mK] – the thermal conductivity
 v_t [m²/s] – the turbulent eddy viscosity
 σ_t [-] – the turbulent Prandtl number

The turbulent heat flux in the energy equation is calculated based on the simple gradient diffusion hypothesis with a constant turbulent Prandtl number of $\sigma_t = 0.85$ [-].

The pressure-velocity coupling was based on the SIMPLE algorithm with the PRESTO! scheme for the discretization of pressure, and the QUICK scheme for the momentum, velocity, turbulence and energy equations. The properties of the air filling the cavity were calculated as temperature dependent (see Table 2).

Table 2 Material properties

property	symbol	value
density	ρ	incompressible ideal gas
specific heat capacity	c_p	1005 [J/kgK] constant
thermal conductivity	λ	piecewise linear interpolation: $\lambda_{T=288.75 \text{ [K]}} = 0.0253$ [W/mK] $\lambda_{T=308.30 \text{ [K]}} = 0.0268$ [W/mK] $\lambda_{T=327.85 \text{ [K]}} = 0.0283$ [W/mK]
dynamic viscosity	μ	acc. the Sutherland formula
molecular mass	M_w	28.97 [g/mol]

The geometry was defined to match the cavity of the experimental apparatus of Betts and Bokhari, and the boundary conditions were chosen to correspond to the higher Rayleigh number of their measurements (see Fig. 3). The vertical walls were isothermal, with $T_{\text{cold}}=288.75$ [K] and $T_{\text{hot}}=327.85$ [K]. This gives a Rayleigh number based on cavity thickness and $T_m=(T_{\text{hot}}+T_{\text{cold}})/2=308.3$ [K] of $Ra=1.43e6$ [-]. The top and bottom walls were defined as either adiabatic (a simplification found in many of the publications) or with a temperature profile taken from the perimeter-thermocouple measurements of Betts and Bokhari (2000).

A mesh refinement study was made and based on the literature research; the effect of both the near wall and the longitudinal

(vertical) mesh resolution was investigated. The effect of near wall resolution was <1% between $y^+=1$ and $y^+=0.035$ [-]. The longitudinal mesh resolution was also increased. In the end, non-uniform rectangular mesh with a constant $dy=10$ [mm] vertical resolution for 90% of the cavity height was adapted with the same boundary layer refinement for the vertical and top/bottom horizontal surfaces.

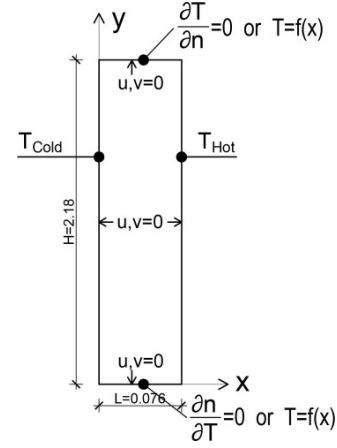


Fig. 3 The cavity geometry and boundary conditions

3 Model validation

The calculation results for all the turbulence models investigated are presented in Figs. 4-7 for the temperature and Figs. 8-9 for the vertical velocity fields.

The low-Re k-ε models give the worst results for both the temperature and velocity fields. They predict excessive vertical temperature stratification at the bottom ($y/H<0.3$) and top ($y/H>0.7$) portions and near zero in the middle ($0.3<y/H<0.7$) of the cavity. They also underpredict the maximum vertical velocities in the boundary layers and with the exception of the Launder-Sharma (1974) model, cannot reproduce the shape of the velocity distribution in the middle of the cavity. The RNG and realizable k-ε models give nearly identical results for both temperature and velocity. Their prediction of the temperature distribution is quite good, especially for the vertical temperature profile across the middle of the cavity; however, they overpredict the maximum velocities and fail to reproduce the correct shape of the velocity profile, much like the low-Re k-ε models.

The best results are obtained with the k-ω SST and v2f models, though the v2f model severely overpredicts the temperature stratification in the middle of the cavity. The k-ω SST model best predicts the maximum flow velocities and both the v2f and SST models produce a reasonable match for the shape of the velocity profile in the middle of the cavity: antimetric, peak velocity ca. 6-7 [mm] from the walls and a near linear distribution of vertical velocities in between.

In the laminar sublayer immediately adjacent to the cavity walls, heat is only transported in the horizontal direction by thermal diffusion in the fluid (since the wall normal velocity is zero). The local Nusselt number is thus calculated as the ratio

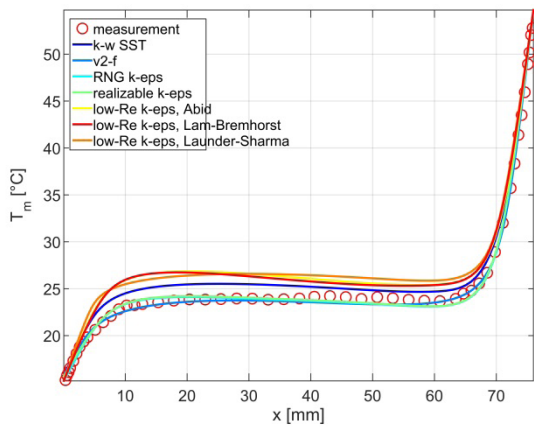


Fig. 4 Horizontal T_m profile at $y/H=0.05$ [-]

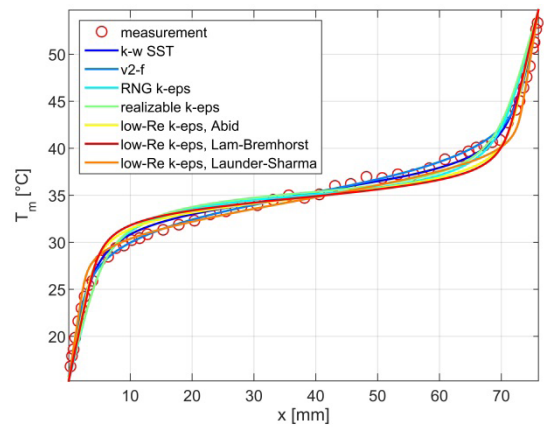


Fig. 5 Horizontal T_m profile at $y/H=0.50$ [-]

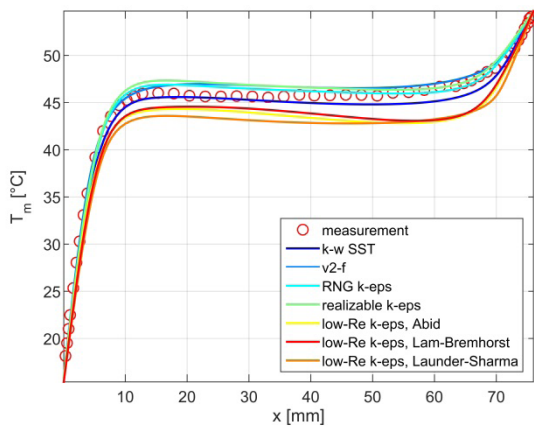


Fig. 6 Horizontal T_m profile at $y/H=0.95$ [-]

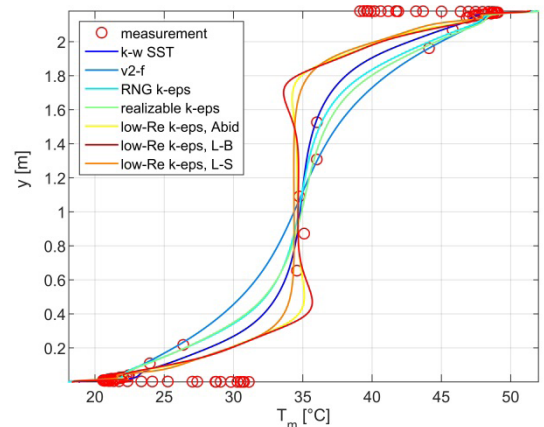


Fig. 7 Vertical T_m profile

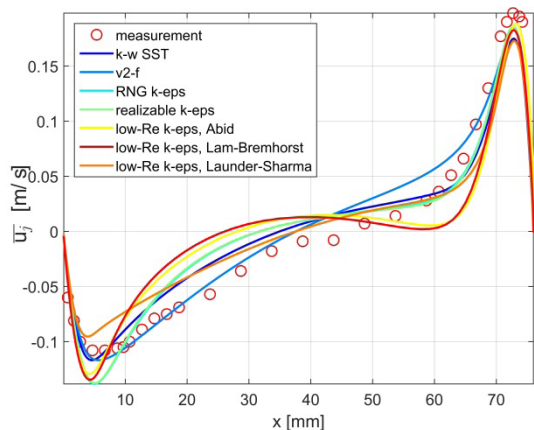


Fig. 8 Horizontal profile of mean vertical velocity at $y/H=0.05$ [-]

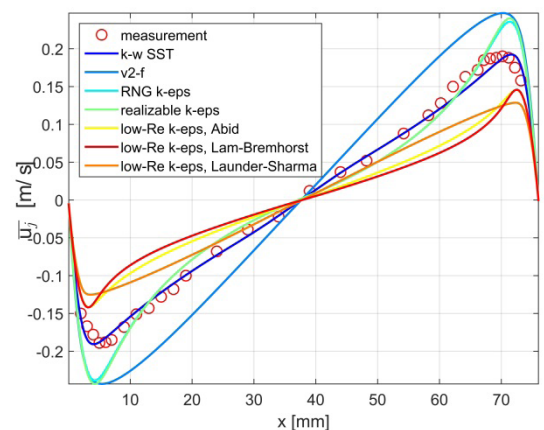


Fig. 9 Horizontal profile of mean vertical velocity at $y/H=0.50$ [-]

between the local surface-normal temperature gradient and a temperature gradient satisfying the Laplace equation (heat flux only by thermal diffusion, i.e. heat conduction in an imaginary stagnant fluid):

$$Nu_{local} = L \frac{\partial T_m}{\partial x} / \Delta T \quad (5)$$

where: Nu_{local} [-] – the local Nusselt number

L [m] – the total thickness of the cavity
 T_m [K] – the mean temperature
 ΔT [K] – the total temperature difference between the hot and cold sides

The average Nusselt number is calculated by taking the surface integral of the local Nusselt number and dividing it by the total cavity height:

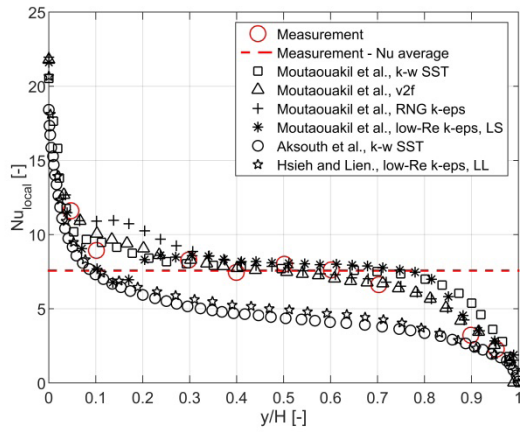


Fig. 10 Horizontal T_m profile at $y/H=0.05$ [-]

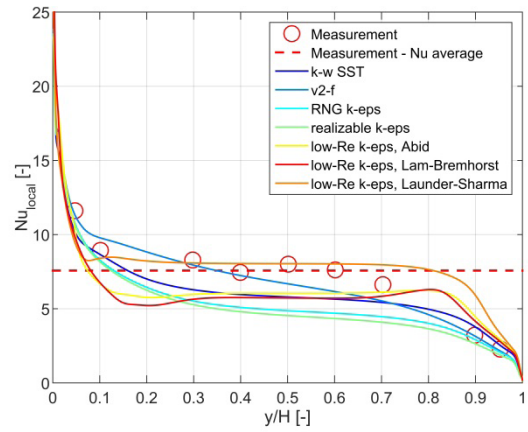


Fig. 11 Local Nusselt number (cold side) - in literature

$$Nu = \frac{1}{H} \int_0^H Nu_{local} dy \quad (6)$$

where: Nu [-] – the Nusselt number
 Nu_{local} [-] – the local Nusselt number
 H [m] – the total height of the cavity

The distributions of the local Nusselt number along the cooled vertical wall of the cavity found in the literature are shown in Fig. 10, the calculated distributions in Fig. 11. The measured local and average Nusselt values reported by Betts and Bokhari are shown in both graphs. The best match of the measurements is clearly found in El Moutaouakil et al. (2014) with all of their turbulence models shown in Fig. 10 producing a $Nu_{average}$ number within 10% of the measurement. Aksouh et al. published similarly good results but the graph showing the local Nusselt number distribution in their paper is possibly faulty and shows a different result. The low-Re $k-\epsilon$ model of Hsieh and Lien give significantly lower values for the convective heat transfer. The picture is different in the calculations of this current study. All models were found to give a low Nu number compared to Betts and Bokhari (see Table 3.), except for the Launder-Sharma low-Re $k-\epsilon$ model, which however produced erroneous temperature and velocity fields as shown earlier. The lowest number is produced by the RNG and realizable $k-\epsilon$ models. The best match for the average Nusselt number is given by the v2f model, but the shape of the local Nusselt number profile is clearly showing the effect of the model's faulty overprediction of vertical temperature stratification. For the $k-\omega$ SST model, the shape of the local Nusselt number's distribution along the cavity wall is consistent with the data, but the calculated average Nusselt number is 19.1% lower than measured.

The reason for the discrepant Nusselt number results, despite the very similar calculated temperature fields, is to be found in the wall adjacent temperature boundary layer. The first 7 [mm] of the calculated temperature field at $y/H=0.5$ [-] along the cold wall, as well as the calculated wall-normal temperature gradients

at the same place, are found in Fig. 12 and 13. In the first ca. 2-3 [mm], the measured and calculated temperature profiles are near linear indicating that we are in the viscous sublayer. While the temperature fields are very similar, according to Eq. (5), the heat flux is proportional to the temperature gradient. The calculated temperature gradients next to the wall and the thickness' of the laminar sublayer are very different depending on the turbulence model. In Betts and Bokhari (1996), the Nusselt number was also calculated from the wall adjacent temperature gradient, and the average $\partial T/\partial n$ was reported as 3900 [K/m]. There were about 11 temperature measurement points in the first 7 [mm] of the boundary layer. The exact value of the temperature gradient is hard to determine from the data they published. For their study, Betts and Bokhari used a fourth order polynomial fitted to the temperature measurement points, and the gradient was determined from this with a claimed accuracy of $\pm 5\%$.

Table 3 The calculated average Nusselt numbers

turb. model	Nu	%Error comp. to Betts and Bokhari ($Nu=7.57$)
$k-\omega$ SST	6.1192	-19.16%
v2f	6.8036	-17.66%
RNG $k-\epsilon$	5.4335	-28.22%
realizable $k-\epsilon$	5.1666	-31.76%
low-re $k-\epsilon$, A	6.2361	-17.16%
low-re $k-\epsilon$, L-B	5.9629	-21.23%
low-re $k-\epsilon$, L-S	7.8005	+3.05%

It is not clear why the calculations of El Moutaouakil et al. and Ammour et al. produced significantly higher Nu numbers with the $k-\omega$ SST model than the current study. The use of the $k-\omega$ SST model in FLUENT with an incompressible ideal gas treatment of buoyancy and temperature dependent material properties is generally known to give good results for convective heat transfer. El Moutaouakil used a proprietary code and

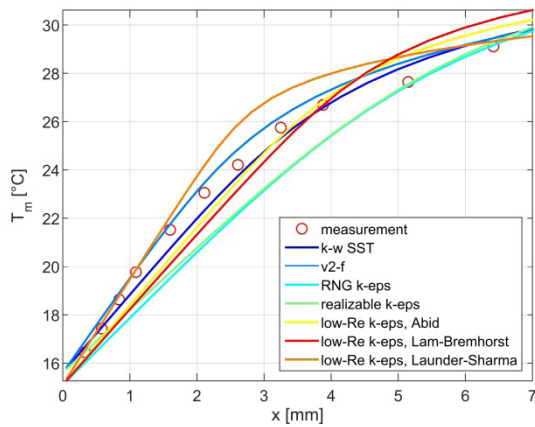


Fig. 12 Temperature field normal to the cold wall at $y/H=0.5$ [-]

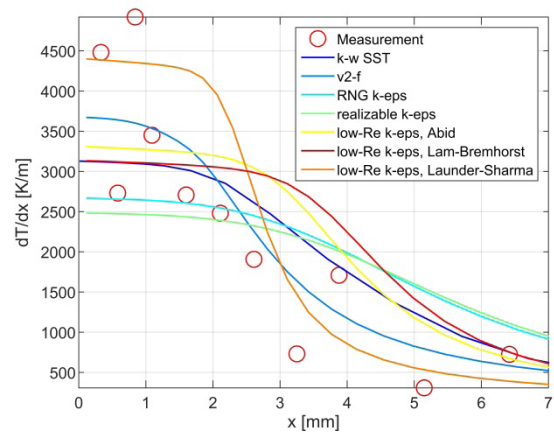


Fig. 13 Temperature gradient normal to the cold wall at $y/H=0.5$ [-]

Table 4 The A and Ra number range of the parameter study

	A [-]									
	7	8.37	10	12	14.3	17.1	20	24.5	29.3	35
Ra_{low} [-]	3e6	2e6	1e6	7e5	6e5	6e5	6e5	6e5	6e5	6e5
Ra_{high} [-]	3e7	2e7	3e7	3e7	3e7	3e7	2e7	1e7	5e6	3e6

Ammour et al. a different CFD software (Code-Saturn) but neither paper mentioned any modifications to the governing equations or the turbulence model constants. Mesh refinement studies for the problem all show very little effect for y^+ below 1, so it is doubtful that the different computational meshes could be the culprit. The material properties and turbulent Prandtl numbers, which could account for the different result, are not published in either one of the papers cited in Table 1. The calculated wall-normal temperature gradients are likewise unreported.

As Betts and Bokhari's setup could not measure the heat flux densities directly (e.g. by thermopiles or by metering the heating and cooling loads) and used temperature measurements instead, there is still sufficient uncertainty to conclude which model is the most accurate. Further study is needed to resolve the differences between the measurements, the published results and the CFD simulations. For the time being, we will keep using the $k-\omega$ SST model as it performed best for both temperature and velocity fields. A study of a wider range of flows must be performed to enable a comparison with the rest of the literature reviewed in part 1 of this article.

4 Parameter study – simple cavity

To cover the range of flows encountered in the cavities of box type windows, a parameter study with 10 times 10 simulations was set up as shown in Fig. 14. The cavity aspect ratio was varied from 7 to 35 [-], and for each aspect ratio, the Rayleigh number, based on cavity thickness, was varied logarithmically between the lowest and a highest value according to Table 4. The prescribed cavity surface temperatures were calculated to give the specified

Ra number with the cavity thickness and a mean temperature of 283.15 [K]. The boundary conditions were set according to Fig. 2, with isothermal vertical walls and adiabatic top and bottom walls.

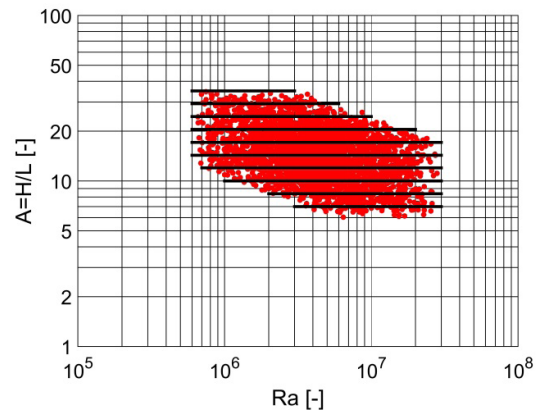


Fig. 14 The typical flow regime in cavities of box type windows (indicated with pairs of Ra and A numbers) and the range of the current study

Fig. 15 shows the distribution of the dimensionless temperature in the cavities of different aspect ratios, and Ra numbers along horizontal sections at heights of $y/H=0.1$, 0.5 and 0.9 [-]. Fig. 16 displays the temperature profile through the vertical axis of the cavity. The dimensionless temperature is defined as $f=(T-T_{cold})/(T_{hot}-T_{cold})$ [-]. The temperature field is similar in all cases, but there is a strong dependence on the aspect ratio. In cavities with small aspect ratios, the vertical temperature stratification is almost perfectly linear. As A increases, the stratification gets stronger in the top and bottom portions and weaker in the middle two-thirds of the cavity, as was the case in the cavity of

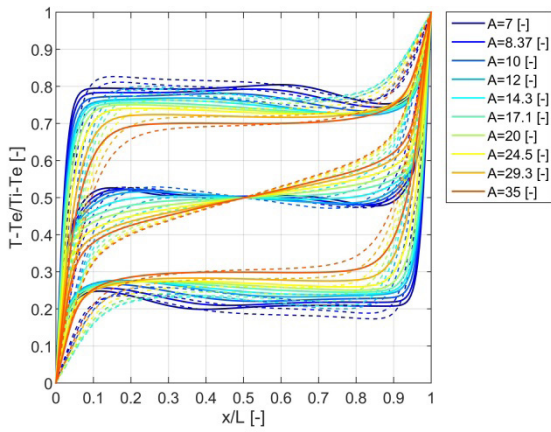


Fig. 15 Horizontal temperature profiles at $y/H=0.1, 0.5$ and 0.9 , for high Ra (solid) and low Ra (dashed) simulations

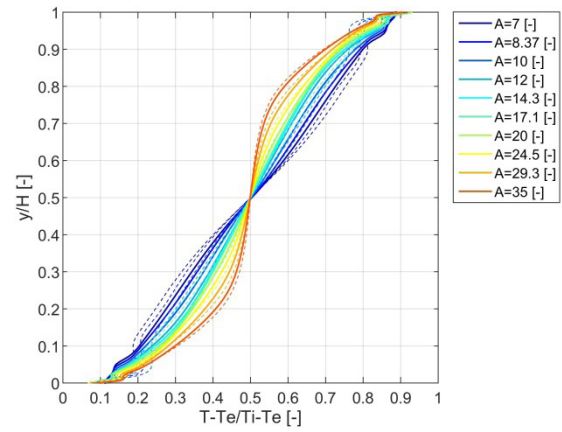


Fig. 16 Vertical temperature profile in the cavity axis for high Ra (solid) and low Ra (dashed) simulations

Betts and Bokhari ($A_{BB}=28.68$ [-]). On the horizontal temperature profiles, the temperature boundary layers are always visible, but the temperature field in the core (between the boundary layers) changes considerably with aspect ratio. For small A 's, there is a near zero horizontal temperature gradient between the boundary layers while in more slender cavities, a distinct linear temperature is observed with about one-fifth of the total temperature difference. The Rayleigh number has a noticeably smaller effect on the temperature field than the aspect ratio. The vertical temperature stratification is almost independent of the Ra number except for the very ends of the cavity. For a lower Ra number, the thickness of the boundary layers is somewhat bigger and consequently the gradient of the dimensionless temperature in the boundary layer is slightly reduced.

The temperature in the core of the cavity outside the boundary layers is well described by the vertical temperature profile in the axis of the cavity. The temperature at the top and the bottom of the cavity is at $f=0.9$ and 0.1 [-], irrespective of the Ra or A number and 0.5 [-] at the middle due to the symmetric nature of the flow. As the temperature stratification is often a key question in the hygrothermal behaviour of box type windows, it is useful to predict this temperature. The following polynomial was created with the help of the nonlinear least squares fit function `lsqnonlin` of MATLAB to give the dimensionless temperature of the core depending on the dimensionless height and aspect ratio:

$$\begin{aligned}
 f = & 0.5 + 0.8963 \times b + 0.0159 \times b^2 - 1.5771 \times b^3 \\
 & - 0.0341 \times b^4 + 5.2452 \times b^5 \dots \\
 & - 0.0238 \times A \times b - 0.0010 \times A \times b^2 + 0.1176 \times A \times b^3 \\
 & + 0.0025 \times A \times b^4 - 0.1282 \times A \times b^5
 \end{aligned} \quad (7)$$

$$b = \left(\frac{y}{H} - 0.5 \right) \quad (8)$$

where: f [-] – the dimensionless temperature of the core
 A [-] – the dimensionless aspect ratio ($A=H/L$)

y [m] – the height
 H [m] – the total height of the cavity

The overall shape of the velocity field (vertical velocity) is also strongly dependent on the aspect ratio, as can be seen in Fig. 17. The velocity field is always antisymmetric with peak values in the boundary layer, but for small aspect ratios, the velocity in the core of the cavity is zero while for larger aspect ratios, there is a near linear distribution of velocities between the two peaks. The maximum vertical velocity for the largest Ra number is between 0.2 and 0.3 [m/s] depending on the aspect ratio. For small Ra numbers, the peak velocities decrease, as expected, but the shape of the velocity profile is not changed. Velocity profiles similar to the measurements of Betts and Bokhari are found only in the large aspect ratio cavities, as was the case with the temperature profiles.

The relative distribution of the surface heat flux along the cold vertical walls of the cavities is shown in Fig. 18. The calculated heat flux densities were “normalized” to give an integrated value of 1 to give a picture of their relative distribution. The convective heat transfer is always strongest at the top edge of the cold wall (and the bottom edge of the warm wall) where the flow inside the cavity loops around. Cavities with a small aspect ratio have a near linearly increasing heat flux density profile from the bottom to the top of the wall, while in more slender cavities, there is a middle, near constant, section where the vertical temperature gradient in the core was shown to be the smallest.

Though all the investigated cavities are in the turbulent boundary layer flow regime, the range of cavity aspect ratios $A=7-35$ [-] represents a transition zone between close-to-rectangular and tall and slender cavities, with different patterns in the temperature stratification and velocity field. In small aspect ratio cavities, the boundary layers resemble those in a square cavity with a horizontally isotherm and vertically stratified core. For larger aspect ratios, the boundary layers begin to interact more and more strongly creating better mixing and less stratification in the core.

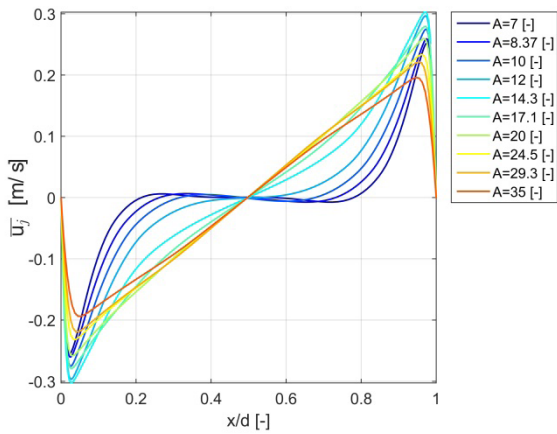


Fig. 17 Horizontal profile of mean vertical velocity at $y/H=0.5$

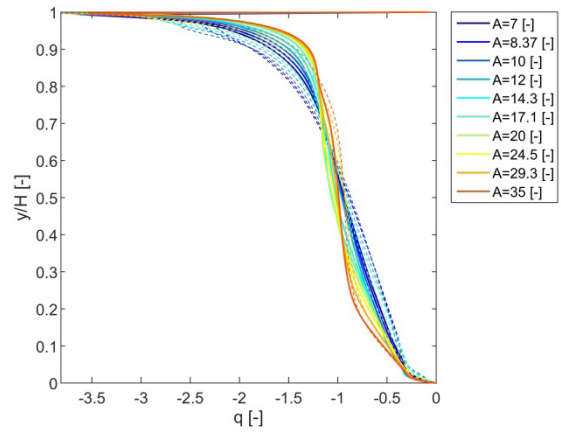


Fig. 18 Relative distribution of heat flux density along the height of the cold cavity wall

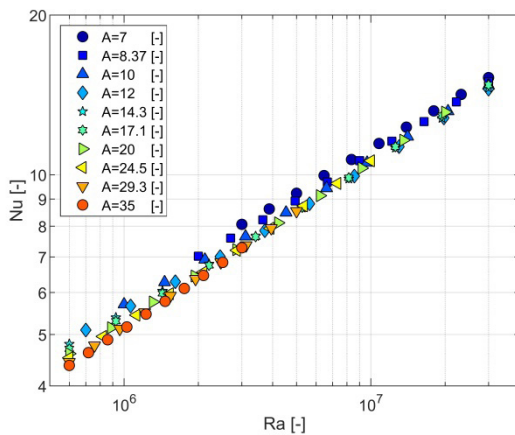


Fig. 19 Calculated Nusselt numbers

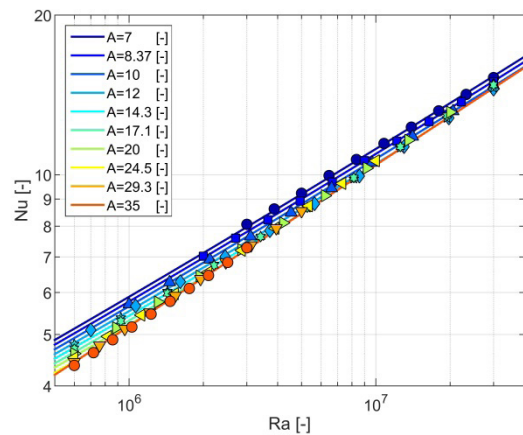


Fig. 20 The new Nusselt number correlation

The average Nusselt numbers calculated are shown in Fig. 19. The Nusselt number is a function of both Ra and A, with bigger aspect ratios producing a smaller Nusselt number for any given Ra, as is expected based on the theory. The effect of A can reach 10-15%. Based on these results, the following new correlation is proposed for calculating the Nusselt number in the cavities of box type windows:

$$Nu = \max \begin{cases} Nu_1 = 0.0776Ra^{0.3041} \\ Nu_2 = 0.01936(1 + Ra^{0.0897}A^{-0.0382})^{3.9826} \end{cases} \quad (9)$$

The correlation (see Fig. 20) is only intended for box type windows, with the A and Ra range of validity clearly set by Table 4. Nu_1 gives the minimum Nusselt number, and it is effective for higher aspect ratios and larger Ra numbers. For a given A, Nu_2 gives $Nu=f(Ra)$ functions with a smaller slope on the double logarithmic graph than Nu_1 that intersects with the latter at larger and larger Ra numbers for lower and lower aspect ratios. This indicates that the aspect ratio becomes more important for smaller Rayleigh numbers. As Ra is increased, the convective heat transfer becomes more and more aspect ratio independent.

The comparison of the new correlation for $A=20$ [-] with others found in the literature (see Part 1 of this article) is shown in Fig. 21. The predicted convective heat transfer is clearly smaller than the standards EN 673 (2011) and ISO 15099 (2003) (and Wright (1996) on which it is based). The nearest match is with the turbulent correlations of Xaman et al. (2005).

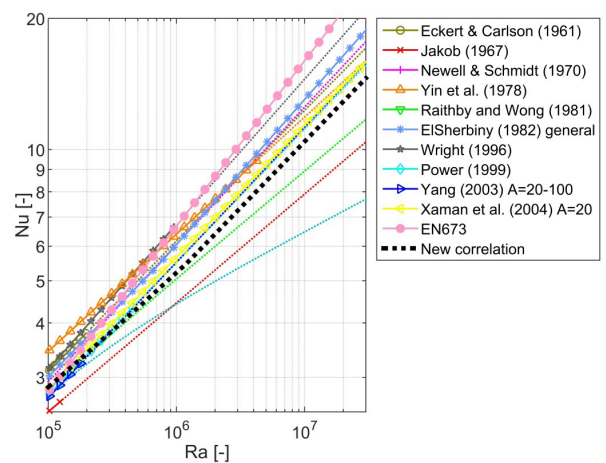


Fig. 21 Comparison of the new correlation for the Nusselt number with the ones found in the literature, for $A=20$ [-] (each correlation is plotted as continuous for its published range of validity and with a dotted line outside the range)

5 Parameters study – simple glazing system

A second parameter study was conducted by modelling the entire simplified representation of the glazing system of box type windows (see Fig. 22). A basic case is a glazing system with a cavity enclosed by two panes of float glass, $t_{gl}=0.003$ [m] thick, on either side. So besides the fluid domain of the cavity, the internal and external solid glazing layers were also added to the model. The aim of this study was to investigate the possible difference in the velocity and temperature field when the boundaries of the cavity are defined, instead of unrealistic isothermal walls, with more realistic glazed surfaces, whose surface temperature is itself a function of the heat transfer processes in the cavity. Furthermore, in many cases, the most important factor in analysing a box type window is the lowest surface temperature in the cavity, since this is the point where moist air, filtering into the window from inside the building, can begin to condense.

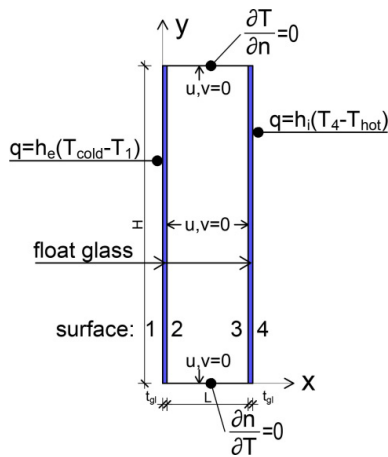


Fig. 22 Schematic representation of the glazing system geometry and boundary conditions

The properties of the glazing material were: $\rho_{gl}=2400$ [kg/m³], $c_{p,gl}=850$ [J/kgK] and $\lambda_{gl}=1$ [W/mK]. As in box type windows, the cavity is formed by the frame itself; no spacers were added for this study. The top and bottom edges were kept as adiabatic, while the cold and hot side boundary conditions were changed from first-type isothermal to a third type boundary with heat transfer coefficients representative for a winter condition: $h_e=25$ [W/m²K] and $h_i=7.6923$ [W/m²K] (see in EN 6946 (2007)). The glazing surfaces are numbered 1 through 4 from the cold to the hot side of the entire glazing system. The internal dimensions of the cavity were defined the same ways as before, while the T_{cold} and T_{hot} temperatures were computed to give the same Rayleigh numbers in the cavity as in Table 4, but calculated based on the average temperatures of the cavity adjacent glazing surfaces – surfaces 2 and 3 instead. This was achieved by running one-dimensional calculations of

the glazing system, based on the ISO 15099 standard (2003), to find the right temperatures.

Due to the addition of the glazing surfaces, an infrared radiation model had to be added to get realistic surface temperatures. The surface-to-surface view factor radiation model of FLUENT was used for the task with a glazing surface longwave infrared emissivity of $\epsilon_{gl}=0.84$ [-] (typical value for uncoated float glass, taken from the International Glazing Database). Radiative heat transfer was only modelled in the cavity. On the external surfaces of the glazing layer, the heat transfer coefficients accounted for both convection and radiation.

The vertical temperature profiles on the number 2 and 3 surfaces as well on the vertical axes of the cavity are shown in Fig. 23. The dimensionless temperature is calculated as $f=T-T_2/(T_3-T_2)$ [-], where T_2 and T_3 are the average surface temperatures of the cavity adjacent glazing surface 2 and 3. As seen in Fig. 23, the temperature stratification of the core is virtually unchanged, while an additional stratification is now visible on the glazing surfaces. The temperature of surface 2 ranges from -0.1 to 0.1 [-], i.e. it can reach a 10% lower or higher temperature between T_{cold} and T_{hot} as the surface average T_1 . On the warm side of the cavity, the stratification is larger: between 0.85 and 1.2 [-]. It is obvious that due to the stratified turbulent boundary layer flow in such windows, the critical surface temperatures cannot be determined by one-dimensional glazing heat transfer simulations only.

The amplitude of the surface temperature stratification is clearly a function of the heat transfer coefficient. A larger heat transfer coefficient (smaller heat transfer resistance) limits the stratification compared to a smaller one. The effect of the surface emissivity was not investigated at this point, but it is reasonable to assume that a low emissivity coating on one side of the cavity and the resulting drop in radiative heat transfer would increase the surface temperature stratification.

As in the simple cavity, the Rayleigh number has only a limited effect on the temperature field, while the cavity aspect ratio is influential in determining not just the core temperature stratification but the surface temperature stratification as well. Lower aspect ratio cavities have a near linear temperature profile between the coldest and hottest surface temperatures, while slender cavities are characterized by a distinct S-shape in the profile. The absolute minimum and maximum temperatures are A independent, but show a larger variance for the very low Ra numbers. Fortunately, surface temperatures are only crucial when the external temperature is low, and the total temperature difference and the cavity Ra number are high.

As expected, the convective heat transfer in the cavity (subtracting the radiative heat transfer from the total heat transfer) was unchanged when compared to the simplified cavity modelled without the glazing system (for the same A and cavity Ra number).

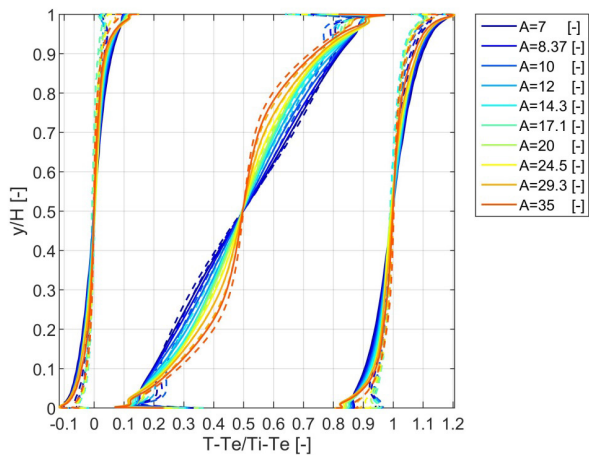


Fig. 23 Horizontal temperature profile in the cavity

6 Conclusions

Two-dimensional steady computational fluid dynamics simulations models were built to study the convective heat transfer in and the temperature and velocity fields of the cavities of box type windows. Although the precise convective heat transfer predictions of the model could not be entirely validated, the $k-\omega$ SST turbulence model of Menter (1994) was found to give good results for the overall temperature and velocity field when compared to the benchmark measurements of Betts and Bokhari (2000).

A parameter study of 100 data points over the entire cavity aspect ratio and Rayleigh number range of box type window cavities gave new insights into the types of natural convection found in these constructions. Although the flow is always in the turbulent boundary layer regime, large differences can be observed between small and large aspect ratio cavities when observing the details of the temperature field, cavity stratifications and velocity fields. Small aspect ratios are characterized by distinct boundary layers, a near zero mean velocity core, and a linear vertical temperature stratification, while more slender cavities have strongly interacting boundary layers and as a result, limited stratification. The cavities of box type windows thus lie midway between the much slender insulating glass units of contemporary windows, and the near square cavities, which are not studied by many authors focusing on researching glazing heat transfer.

As the convective heat transfer and the Nusselt number in the cavity was found to be a function of both Rayleigh number and aspect ratio, a new correlation is proposed to capture this dependence. This new equation is intended to be used only for the cavities of box type windows, and it predicts a smaller convective heat transfer than the ones used in the two glazing heat transfer calculation standards most used today (EN673 (2011) and ISO 15099 (2003)).

With another parameter study of a complete, albeit simplified, glazing system, it was demonstrated that the vertical temperature stratification in the core of the cavity also causes significant temperature stratification in the glazing surface

temperatures. This has to be incorporated into calculations aimed at studying the condensation resistance of box type windows. The results of this article could prove useful for predicting the lowest glazing surface temperatures, although further study is still needed to investigate the effects of more of the influencing parameters (glazing surface emissivity, internal and external heat transfer coefficients).

Acknowledgements

We thank Árpád Veress at the Budapest University of Technology and Economics, Department of Aeronautics, Naval Architecture and Railway Vehicles for his advice and support for the CFD simulations.

References

- Abid, R. (1993). Evaluation of two-equation turbulence models for predicting transitional flows. *International Journal of Engineering Science*. 31(6), pp. 831-840. [https://doi.org/10.1016/0020-7225\(93\)90096-D](https://doi.org/10.1016/0020-7225(93)90096-D)
- Aksouh, A., Mataoui, A., Seghouani, N., Haddad, Z. (2010). Assessment of performance of low Reynolds turbulence models in predicting natural convection. In: V. European Conference on Computational Fluid Dynamics ECCOMAS CFD 2010. Pereira, J. C. F., Sequeira, A. (eds.), Lisbon, Portugal, June 14-17, 2010.
- Aksouh, A., Mataoui, A., Seghouani, N., Haddad, Z. (2011). Rayleigh number effect on the turbulent heat transfer within a parallelepiped cavity. *Thermal Science*. 15(Suppl. 2), pp. 341-356. <https://doi.org/10.2298/TSCI110201114A>
- Ammour, D., Iavocides, H., Craft, T. J. (2011). Model validation of buoyancy-driven flows inside differentially heated cavities. In: Proceedings of the 12th UK National Heat Transfer Conference, Leeds, UK.
- ANSYS FLUENT Theory Guide (2010). Release 13.0, ANSYS, Inc. Southpointe, USA <http://www.ansys.com>
- Betts, P. L., Bokhari, I. H. (2000). Experiments on turbulent natural convection in an enclosed tall cavity. *International Journal of Heat and Fluid Flow*. 21(6), pp. 675-683. [https://doi.org/10.1016/S0142-727X\(00\)00033-3](https://doi.org/10.1016/S0142-727X(00)00033-3)
- Chen, Q., Xu, W. (1998). A zero-equation turbulence model for indoor airflow simulation. *Energy and Buildings*. 28(2), pp. 137-144. [https://doi.org/10.1016/S0378-7788\(98\)00020-6](https://doi.org/10.1016/S0378-7788(98)00020-6)
- Dafa'Alla, A. A., Betts, P. L. (1996). Experimental study of turbulent natural convection in a tall air cavity. *Experimental Heat Transfer*. 9(2), pp. 165-194. <https://doi.org/10.1080/08916159608946520>
- Davidson, L., Nielsen, P. V., Sveningsson, A. (2003). Modification of the V2-f model for computing the flow in a 3d wall jet. *Turbulence Heat and Mass Transfer*. 4, pp. 577-584.
- Durbin, P. A. (1995). Separated Flow Computations with the $k-\epsilon-v_2$ Model. *AIAA Journal*. 33(4), pp. 659-664. <https://doi.org/10.2514/3.12628>
- Eckert, E. R. G., Carlson, W. O. (1961). Natural convection in an air layer enclosed between two vertical plates with different temperatures. *International Journal of Heat and Mass Transfer*. 2(1-2), pp. 106-120. [https://doi.org/10.1016/0017-9310\(61\)90019-9](https://doi.org/10.1016/0017-9310(61)90019-9)
- El Moutaouakil, L., Zrikem, Z., Abdelbaki, A. (2014). Performance of various RANS eddy-viscosity models for turbulent natural convection in tall vertical cavities. *Heat and Mass Transfer*. 50(8), pp. 1103-1113. <https://doi.org/10.1007/s00231-014-1322-4>
- ElSherbiny, S. M., Hollands, K. G. T., Raithby, G. D. (1982a). Effect of thermal boundary conditions on natural convection in vertical and inclined air layers. *Journal of Heat Transfer*. 104(3), pp. 515-520. <https://doi.org/10.1115/1.3245123>

- ElSherbiny, S., Hollands, K., Raithby, G. (1982b). Effect of the Thermal Boundary Condition on Natural Convection in Vertical and Inclined Air Layers. In: *Transaction of the ASME*, July 27-30, 1982, pp. 96-102.
- EN 673 (2011). Glass in building. Determination of thermal transmittance (U value). Calculation method.
- EN 6946 (2007). Building components and building elements. Thermal resistance and thermal transmittance. Calculation method.
- European Research Community on Flow, Turbulence and Combustion Database. http://cfd.mace.manchester.ac.uk/cgi-bin/cfd/db/prpage.cgi?79&EXP&database/cases/case79/Case_data&database/cases/case79&cas79_head.html&cas79_desc.html&cas79_meth.html&cas79_data.html&cas79_refs.html&cas79_rsol.html&1&0&0&0&0
- Ganguli, A. A., Pandit, A. B., Joshi, J. B. (2009). CFD simulation of heat transfer in a two-dimensional vertical enclosure. *Chemical Engineering Research and Design*. 87(5), pp. 711-727. <https://doi.org/10.1016/j.cherd.2008.11.005>
- Gibson, M. M., Launder B. E. (1978). Ground Effects on Pressure Fluctuations in the Atmospheric Boundary Layer. *Journal of Fluid Mechanics*. 86(3), pp. 491-511. <https://doi.org/10.1017/S0022112078001251>
- Hsieh, K. J., Lien, F. S. (2004). Numerical modeling of buoyancy-driven turbulent flows in enclosures. *International Journal of Heat and Fluid Flow*. 25(4), pp. 659-670. <https://doi.org/10.1016/j.ijheatfluidflow.2003.11.023>
- ISO 15099 (2003). Thermal performance of windows, doors and shading devices - Detailed calculations.
- Kayne, A., Agarwal, R. K. (2013). Computational fluid dynamics modeling of mixed convection flows in buildings enclosures. *International Journal of Energy and Environment*. 4(6), pp. 911-932.
- Lam, C. K. G., Bremhost, K. (1981). A modified form of the k- ϵ model for prediction of wall turbulence. *Journal of Fluids Engineering*. 103(3), pp. 456-460. <https://doi.org/10.1115/1.3240815>
- Launder, B. E., Sharma, B. I. (1974). Application of the energy dissipation model of turbulence to the calculation of flow near a spinning disc. *Letters in Heat and Mass Transfer*. 1(2), pp. 131-137. [https://doi.org/10.1016/0094-4548\(74\)90150-7](https://doi.org/10.1016/0094-4548(74)90150-7)
- Lee, Y., Korpela, S. A. (1983). Multicellular Natural Convection in a Vertical Slot. *Journal of Fluid Mechanics*. 126, pp. 91-121. <https://doi.org/10.1017/S0022112083000063>
- Lien, F. S., Leschziner, M. A. (1999). Computational modeling of a transitional 3D turbine-cascade flow using a modified low-Re k- ϵ model and a multi-block scheme. *International Journal of Computational Fluid Dynamics*. 12, pp. 1-15. <https://doi.org/10.1080/10618569908940812>
- Menter, F. R. (1994). Two-Equation Eddy-Viscosity Turbulence Models for Engineering Applications. *AIAA Journal*. 32(8), pp. 1598-1605. <https://doi.org/10.2514/3.12149>
- Newell, M. E., Schmidt, F. W. (1970). Heat Transfer by Laminar Natural Convection Within Rectangular Enclosures. *Journal of Heat Transfer*. 92(1), pp. 159-167. <https://doi.org/10.1115/1.3449616>
- Raitby, G. D., Wong, H. H. (1981). Heat transfer by natural convection across vertical air layers. *Numerical Heat Transfer*. 4(4), pp. 447-457. <https://doi.org/10.1080/01495728108961803>
- Shewen, E., Hollands, K. G. T., Raithby, G. D. (1996). Heat Transfer by Natural Convection Across a Vertical Air Cavity of Large Aspect Ratio. *Journal of Heat Transfer*. 118(4), pp. 993-995. <https://doi.org/10.1115/1.2822603>
- Wright, J. L., Sullivan, H. F. (1993). Natural Convection in Sealed Glazing Units: A Review. *ASHRAE Transactions*. 99(2), pp. 1193-1206.
- Wright, J. (1996). A Correlation to Quantify Convective Heat transfer Between Vertical Window Glazings. *ASHRAE Transactions*. 102, pp. 940-946.
- Xaman, J., Álvarez, G., Lira, L., Estrada, C. (2005). Numerical study of heat transfer by laminar and turbulent natural convection in tall cavities of façade elements. *Energy and Buildings*. 37(7), pp. 787-794. <https://doi.org/10.1016/j.enbuild.2004.11.001>
- Yakhot, V., Orszag S. A. (1986). Renormalization group analysis of turbulence: Part I: Basic theory. *Journal of Scientific Computing*. 1(1), pp. 3-51. <https://doi.org/10.1007/BF01061452>
- Yin, S. H., Wung, T. Y., Chen, K. (1978). Natural convection in an air layer enclosed with rectangular cavities. *International Journal of Heat and Mass Transfer*. 21(3), pp. 307-315. [https://doi.org/10.1016/0017-9310\(78\)90123-0](https://doi.org/10.1016/0017-9310(78)90123-0)
- Zhai, Z. J., Zhang, Z., Zhang, W., Chen, Q. Y. (2007a). Evaluation of Various Turbulence Models in Predicting Airflow and Turbulence in Enclosed Environments by CFD: Part-1: Summary of Prevalent Turbulence Models. *HVAC & R Research*. 13(6), pp. 853-870. <https://doi.org/10.1080/10789669.2007.10391459>
- Zhang, Z., Zhang, W., Zhai, Z. J., Chen, Q. Y. (2007b). Evaluation of Various Turbulence Models in Predicting Airflow and Turbulence in Enclosed Environments by CFD: Part-2: Comparison with Experimental Data from the Literature. *HVAC & R Research*. 13(6), pp. 871-886. <https://doi.org/10.1080/10789669.2007.10391460>
- Zhao, Y., Goss, W. P., Curcija, D. (1997). Prediction the Multicellular Flow Regime of Natural Convection in Fenestration Glazing Cavities. *ASHRAE Transactions*. 103(1), pp. 1009-1020.